Dyes and Pigments 173 (2020) 107964

Contents lists available at ScienceDirect

Dyes and Pigments

journal homepage: http://www.elsevier.com/locate/dyepig

2-Phenylbenzothiophene-based liquid crystalline semiconductors

Yu-Jie Zhong [a], Ke-Qing Zhao [a,***], Bi-Qin Wang [a], Ping Hu [a], Hirosato Monobe [b,**], Benoît Heinrich [c], Bertrand Donnio [c,*]

[a] College of Chemistry and Material Science, Sichuan Normal University, Chengdu, 610066, China
[b] Inorganic Functional Materials Research Institute, National Institute of Advanced Industrial Science and Technology (AIST), Ikeda, Osaka, 5638577, Japan
[c] Institut de Physique et Chimie des Matériaux de Strasbourg (IPCMS), CNRS-Université de Strasbourg (UMR 7504), 67034, Strasbourg, France

ARTICLE INFO

Keywords:
Organic semiconductor
Time-of-flight photocurrent technique
2-Phenylbenzothiophene
Smectic mesophase

ABSTRACT

We report herein the design and synthesis of some novel liquid crystalline semiconductors constructed from a biologically and pharmacologically active building block molecule, namely 6-methoxy-2-(4-methoxyphenyl) benzo[b]thiophene, presenting efficient luminescence and medium charge mobility rate. A first series of mesogenic 2-phenylbenzothiophene derivatives (*n*PBT) was simply and rapidly obtained in good yields by successive demethylation/alkylation reactions of the available methoxy precursor. The further stepwise oxidations moreover resulted in two new sets of the corresponding sulfoxide (*n*PBTO) and sulfone (*n*PBTO$_2$) derivatives, respectively, that were also mesomorphic. The liquid crystalline behaviour was comprehensively characterized by DSC, POM and SAXS: all compounds exhibit smectic-like behaviour in agreement with their calamitic shape. More specifically, mesogens *n*PBT showed a SmA phase, with in addition, a higher ordered smectic phase at lower temperature. As for the oxidized mesogens, they displayed a SmA phase only, and over particularly large temperature ranges for the *n*PBTO with longer chain lengths ($n \geq 8$). The photo-physical properties have also been studied both in solution and thin films, and the molecules were found to display strong absorption in the UV/vis domain and intense luminescence in the range of 400–650 nm (yellowish green light) in high quantum yields (up to 62%). Both absorption and luminescence were also found to be affected by the oxidation of the benzothiophene moiety. Finally, the semi-conducting behaviour of three PBT compounds in the various mesophases was investigated by photocurrent TOF technique. Hole mobility rates of ca. 4×10^{-3} cm^2 V^{-1} s^{-1} were measured in the lower temperature ordered mesophase for all of them, with the best performances (temperature range and mobility values) however obtained for the shortest homolog ($n = 6$). With such highly reasonable mesomorphic, light-emitting and semiconducting functional features, as well as being cheap and easy to synthesize and to process, these materials become very attractive and may be incorporated into various kinds of electronic devices (OFET and OLED).

1. Introduction

The benzo[*b*]thiophene core exhibits a wide range of biological and pharmacological activities thanks to structural similarities with many natural and synthetic molecules in drug design [1]. For instance, the 2-phenylbenzo[*b*]thiophene motif is the main parent structure of cancer drugs like raloxifene and arzoxifene [2], and it is also used in the treatment of Alzheimer's disease [3]. Benzothiophene and its derivatives have now became indispensable building blocks for chemistry and for the development of the drug industry as it has been found to possess many more biological activities [1].

Therefore, as important pharmaceutical intermediate, it is produced in large scale, and thus is abundant, cheap and widely commercially available. However, despite this economical advantage, its natural rod-like shape, easy synthetic derivatization and appealing electronic structure, 2-phenylbenzo[*b*]thiophene has not yet been considered in the design of liquid crystalline materials with potentially interesting semiconducting behaviour.

Thiophene-containing liquid crystalline (LC) semiconductors (Fig. 1) perform a high degree of π-delocalization and optical tunability due to

* Corresponding author.
** Corresponding author.
*** Corresponding author.
E-mail addresses: kqzhao@sicnu.edu.cn (K.-Q. Zhao), monobe-hirosato@aist.go.jp (H. Monobe), bdonnio@ipcms.unistra.fr (B. Donnio).

https://doi.org/10.1016/j.dyepig.2019.107964
Received 12 September 2019; Received in revised form 11 October 2019; Accepted 11 October 2019
Available online 12 October 2019

the combination of their intermolecular well-ordered morphology and unique electronic structure, which is an essential requirement for applications involving optoelectronic and photonic devices [4–9]. In addition, such materials usually show good charge carrier mobility, which depends strongly on the degree of ordering of the self-organized mesophases and on the orientation of the LC molecules, indicating the promising prospects of thiophene-based organic semiconductors for realizing cheap, flexible and printed electronics applications [10–14]. Among the promising thiophene-based candidates for OFETs are the benzothienobenzothiophene (BTBT) derivatives (Fig. 1) [15–18]. The core of BTBT consists of two fused benzothiophene motifs and due to the presence of lateral aliphatic chains, the corresponding molecules present good solubility in organic solvents as well as form well-ordered crystalline thin films, resulting in high carrier mobility [19–22]. Recently, our group has reported such BTBT-based semiconductors containing disk and calamitic LC molecules, which exhibit bipolar carrier mobility in the range of 10^{-3} $cm^2 V^{-1} s^{-1}$ in the columnar mesophase, and carrier mobility of hole approaching 0.07 $cm^2 V^{-1} s^{-1}$ in the smectic phase, as measured by TOF technique [23,24]. Today, a large range of new thiophene-containing semiconductors of various shapes and structures, and differing in the sequences and connections between the thiophene units, are being investigated and their semiconducting performances evaluated in ordered mesophases (Fig. 1). Charge mobilities higher than 10 $cm^2 V^{-1} s^{-1}$ [25–28], have been achieved with various thiophene-based LC materials, even in solution process [29,30], proving that they are expected to be promising materials to display good OTFTs device performances.

However, some economic constraints and environmental drawbacks need to be tackled and considered in this active field of research. First, from a synthetic view point, the chemistry of such organic semiconducting molecules is usually not straightforward, and often requires metal-catalysed coupling methods for connecting the different active parts through polluting, metal-contamination, expensive, time-consuming and sometimes low-yields synthetic procedures [31]. Thus, the easy access to an abundant precursor resource is always beneficial and cost- and time-saving in materials science, especially to carry out systematic studies on structure-property relationships. Secondly, the other fundamental prerequisite that drives the good functioning of the organic devices, and which has been extensively investigated in LC materials, is the ability to prepare high quality organic thin crystalline films (defect-free), with good molecular orientation, either as-deposited

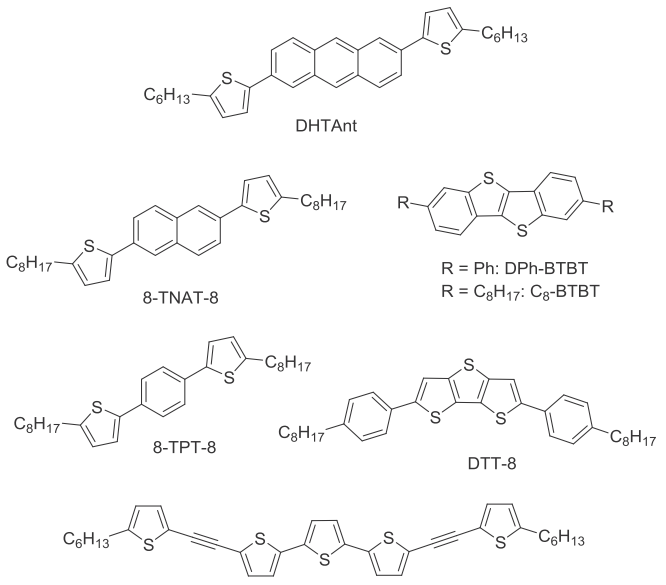

Fig. 1. Representative thiophene-based LC semiconductors reported in the literature.

or after thermal annealing of the liquid crystal phase, leading to effective charge carrier transport in organic field-effect transistors (OFETs) [32–38]. Thus, since they combine features of both crystalline and amorphous materials, the molecular design of novel LC semiconductors, supported by time-saving and efficient synthetic strategies, is highly desirable (self-organization, fluidity, and self-healing abilities, high control of the molecular orientation, one- or two-dimensional charge transport properties) for the discovery of new materials and the modulation of their physical properties. Yet, few works of LC materials consisting of a very simple benzothiophene system have been described in patents and literature, though it has already been proved versatile in the design of various mesogens [39–41].

In this work, a series of 2-phenylbenzo[*b*]thiophene (*n*PBT) mesogenic derivatives was synthesized in two easy steps and in good yields from abundant available starting material, *i.e.* 6-methoxy-2-(4-methoxyphenyl)benzo[b]thiophene, which already possesses a natural rod-like and π-conjugated core, prerequisite of LC phase formation and semiconducting behaviour. Further stepwise chemical oxidation of the benzothiophene moiety resulted in two additional sets of functional derivatives, namely the corresponding sulfoxide homologues (*n*PBTO) and one sulfone derivative (10PBTO$_2$), which were also found to be mesomorphous. The liquid crystalline properties, photo-physical behaviour and charge transport properties were influenced greatly by adjusting the length of terminal alkyl chain and by the degree of oxidation of the benzothiophene moiety. All *n*PBT showed a SmA phase in addition to a low-temperature, high-ordered smectic phase, while only a SmA phase was observed for the oxidized derivatives *n*PBTO and 10PBTO$_2$. The photo-physical properties, highly depending on the oxidation degree, displayed strong UV/Vis absorption and intense yellowish green luminescence, with high quantum yields, in the range of 38–62%. The charge transport carrier of three PBT compounds was also precisely measured in various mesophases as a function of chain-length by photocurrent TOF technique, and found to exhibit hole mobility rate of about 4.2×10^{-3} $cm^2 V^{-1} s^{-1}$, in the low temperature ordered mesophase.

2. Results and discussion

2.1. Synthesis and characterization

The synthesis of the benzo[*b*]thiophene derivatives was straightforward, and is shown in Scheme 1. The dihydroxy compound **2** was prepared by demethylation of the readily available precursory compound **1** with pyridine hydrochloride at 190 °C, and obtained as a white solid in almost quantitative yield (87%). Then, Williamson etherification of **2** with *n*-alkylbromide at both ends gave the desired *n*PBT derivatives (white crystalline solids) in 80–92% yields.

The synthesis of the *n*PBTO derivatives was based on the general procedure described in literature, consisting of the oxidation of *n*PBT by addition of trifluoroacetic acid and a 30% aqueous solution of H_2O_2 at 0 °C [42]. The sulfoxide compounds were obtained as yellow-green powders in yields ranging between 50 and 73%. The sulfone derivative 10PBTO$_2$ could be directly obtained from 10PBT in 70% yield, by simply increasing the amount of trifluoroacetic acid and extending the reaction time. It is worth noting that as the alkyl chain-length was increased, the solubility of *n*PBT compounds deteriorated in chloroform, whereas compounds *n*PBTO and 10PBTO$_2$ showed almost the same good solubility. The structures of all synthesized compounds were characterized by means of ^{1}H and ^{13}C NMR (Fig. S11), elemental analysis, and high resolution mass spectroscopy (HRMS, Fig. S12). Details on the synthesis are given in the Supplementary Information.

2.2. Mesomorphic properties

The mesomorphic behaviour of all compounds was investigated by polarized optical microscopy (POM, Fig. S1) and differential scanning

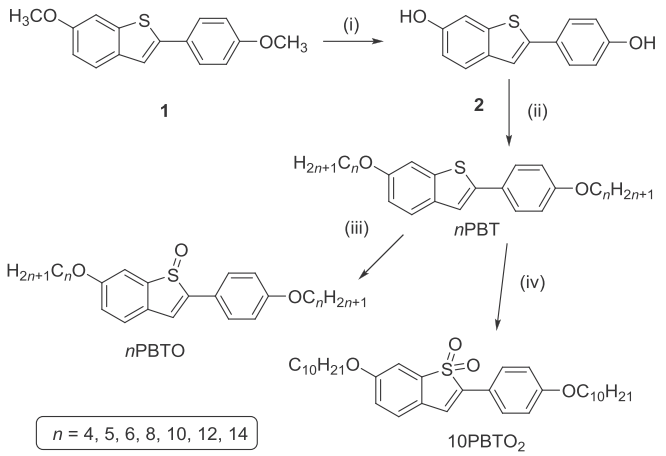

Scheme 1. Synthesis, yields and nomenclature of the benzo[*b*]thiophene derivatives (*n*PBT) and corresponding oxidized homologues (*n*PBTO and $10PBTO_2$). Reagents and conditions: (i) pyridine hydrochloride, reflux, 1 h, 190 °C (87%). (ii) *n*-Bromoalkane, K_2CO_3, 2-butanone, 24 h, 100 °C, (80–92%). (iii) Trifluoroacetic acid, anhydrous CH_2Cl_2, 30% H_2O_2, 2–6 h, 0 °C (50–73%). (iv) Excess of trifluoroacetic acid, anhydrous CH_2Cl_2, 30% H_2O_2, 8 h, 0 °C (70%).

calorimetry (DSC, Fig. S2, Table S1). From POM observations, all the phenylbenzothiophenes and the oxidized derivatives are liquid crystalline and solely show smectic phases consistent with their calamitic shape. The *n*PBT compounds exhibit all a high temperature smectic A (SmA), which was unequivocally recognized by the formation of smooth, focal conic, typical fan-shaped textures, as observed for all of them on slow cooling from the isotropic liquid (Figs. 2 and S1). For two short homologues of this series, an additional phase was also detected by POM and DSC (Figs. S1 and S2, Table S1), monotropic for 5PBT and enantiotropic for 6PBT, assigned as SmB by POM. On further cooling, another less fluid, higher-ordered smectic-like phase was detected, prior to crystallization, by an abrupt textural change with the transformation of the fans and focal conics to a spherulitic texture (Figs. 2 and S2), which is reminiscent of a higher molecular re-organization within the layers [43]. Both *n*PBTO and $10PBTO_2$ showed a single SmA phase (Fig. 2) recognized by the characteristic fan-shaped optical textures. All the transition temperatures were confirmed by DSC (Fig. S2).

With the increase of the alkyl chain-length, the clearing temperature of the *n*PBT terms is decreased (Fig. 3). The range of the SmA phase however expands gradually to ca. 25 °C (maximum SmA range for 10PBT). Meanwhile, the interval of the low-temperature phase (referred to as SmX, see below) decreased at the expense of the expansion of the crystalline phase (Cr). This highly ordered phase has completely disappeared in the longest homolog 14PBT.

The thermal behaviour of the next series is simpler, with the rapid enlargement of the SmA range with the increase of the alkyl chain length to reach a 40 °C range for the longer homologues (maximum SmA range for 10PBTO), due essentially to a smooth decrease of the clearing

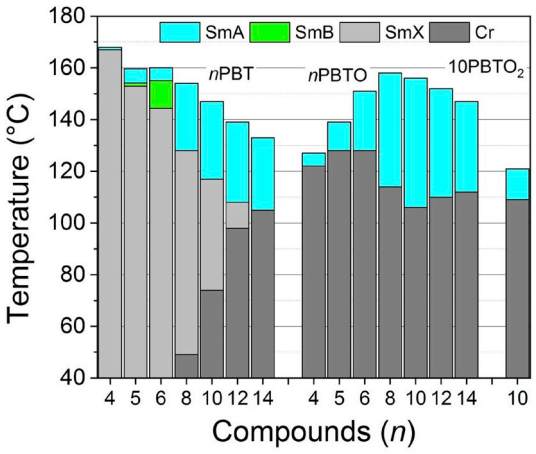

Fig. 3. Bar graph summarizing the thermal behaviour of *n*PBT, *n*PBTO and $10PBTO_2$ derivatives (2nd heating).

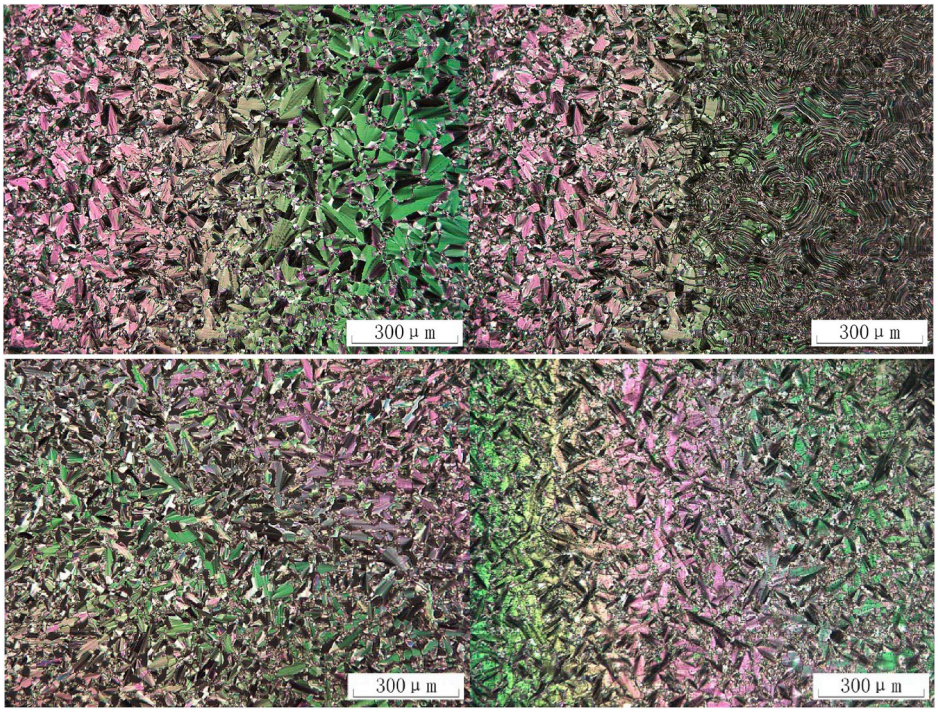

Fig. 2. Representative POM images, observed on cooling from the isotropic liquid: clockwise from top left: 10PBT at 120 °C in SmA; 10PBT at 114 °C in SmX; 10PBTO at 145 °C in SmA; $10PBTO_2$ at 77 °C in SmA.

temperatures (for $n \geq 8$) and an average melting between 100 and 110 °C. The isotropization temperatures of *n*PBTO are higher than of their corresponding *n*PBT homologues ($n \geq 8$), and likely dependent on the stronger dipolar interactions in the latter [44,45]. The reason for the appearance of the highly ordered phase (SmX) in PBT series may be attributed to the presence of the aromatic-rich π-electron system and a strong permanent dipole on the sulfur atom in the thiophene ring, which endows molecules with high anisotropic polarizability and occurrence of spontaneous polarization [46–48]. The electron-withdrawing ability of the sulfur atom in sulfoxide *n*PBTO is stronger than in *n*PBT resulting in the increase of the isotropization temperature. Further oxidation is detrimental to mesophase stability, which, when compared to the two other decyl derivatives, 10PBT and 10PBTO, is reduced down to 10 °C only for $10PBTO_2$, between ca. 110–120 °C.

The smectic nature of the mesophases of all benzo[*b*]thiophene derivatives was confirmed by small-angle X-ray scattering (Figs. 4 and S3, Table S2). On cooling from the isotropic liquid, in the upper temperature phase, most compounds show a single, intense fundamental reflection (001) along a few higher order peaks (002, 003, …), in the ratio 1:2:3: …, characterizing the lamellar arrangement of the molecules, along a diffuse scattering at high Bragg angles, corresponding to the molten chains (Fig. 4, h_{ch}). The SAXS patterns of the *n*PBTO terms, of lesser quality (less peaks and of lower intensity) than those of the *n*PBT series and that of $10PBTO_2$, but still are in agreement with the formation of a smectic phase. Combined with POM, the mesophase can be readily assigned to as SmA in all cases. As expected, the *d*-spacings in the SmA increase almost linearly with the alkyl chain length (Fig. 4) for both series *n*PBT and *n*PBTO, respectively, whereas the molecular area, obtained from the ratio between the molecular volume (V_{mol}) and the smectic periodicity (Table S2), do not greatly vary with *n*, but logically increase upon oxidation of the thiophene ring along the sequence *n*PBT ($A \approx 27.5–30$ Å^2) → *n*PBTO ($A \approx 32.5–35$ Å^2) → nPBTO$_2$ ($A \approx 34.5$ Å^2). Upon further cooling, the SAXS patterns of the PBT terms revealed numerous sharp and equidistant (00*l*) reflections over the whole angular range (up to 13 for 14PBT, Fig. S3) confirming the resilience of the long-range lamellar layering, with very sharp interfaces, which persists even in the lower temperature crystalline phase (Cr). The scattering halo corresponding to the molten chains is no more detectable on the SAXS patterns, suggesting that the chains are in a crystalized or pseudo crystalized state, and thus that the phase is not a true liquid crystalline phase. The supramolecular organizations within the SmX (standing for crystalline phase with a highly well-defined smectic structure) and crystalline (Cr) phases appear very similar to each other (similar spacing) and close to the SmA phase.

2.3. Photophysical properties – UV/Vis absorption and photoluminescence properties

The impact of the oxidation of the thiophene ring on the photophysical properties was evaluated in dilute THF solutions (10^{-5} mol L^{-1}), and in thin films for all benzo[*b*]thiophene derivatives, *n*PBT, *n*PBTO and $10PBTO_2$. The absorption spectra recorded for solutions of *n*PBT exhibit two main absorption maxima at 240 and 320 nm, while for those of *n*PBTO and $10PBTO_2$ showed three strong absorption maxima centred at 235, 305 and 375 nm, and at 252, 312 and 373 nm, respectively (Figs. 5 and S4). Solutions of *n*PBT showed a maximum emission at 365 nm with two shoulder peaks at 350 and 382 nm, and a double maximum emission in thin film, at ca. 372 and 393 nm.

Emission spectra for the solutions of *n*PBTO exhibited one broad emission maximum at 477 nm while centred at 480 nm in thin film, whereas $10PBTO_2$ showed a similar emission maximum slightly shifted at 459 nm in THF solution and at 476 nm in thin film. It is worth noting that *n*PBTO showed yellow-green light emission in THF and thin film under the illumination of UV light of 365 nm (Fig. S4). Quantum yields calculated for *n*PBT were around 50%, slightly lower for *n*PBTO, at around 40%; $10PBTO_2$ exhibited the highest quantum yield with a value

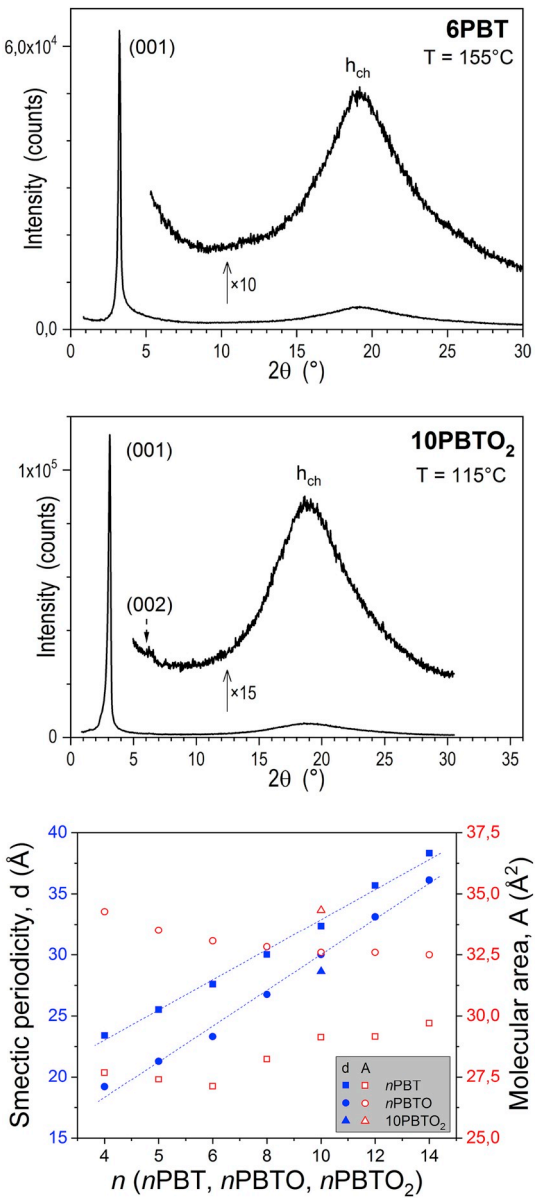

Fig. 4. Two representative SAXS patterns (6PBT, top, and $10PBTO_2$, middle). Variation of the lamellar periodicity, d, and molecular area, A, with the alkyl chain length, *n*, for *n*PBT, *n*PBTO and $10PBTO_2$ derivatives (bottom).

of 62% (Tables 1 and S3). The length of the alkyl chains has almost no influence on the absorption and emission spectra which are fully superimposable (Fig. S4).

2.4. Charge transport properties

Time-of-flight (TOF) technique was used to investigate the charge carrier mobility of the various liquid crystalline materials. For this study, both the hole and negative charge mobilities of three representative benzothiophene derivatives, *n*PBT with $n = 6$, 8, 10, were studied as a function of chain-length. The transient photocurrent decay curves obtained at different temperatures from the isotropic down to the crystalline phase showed reasonable shapes of decay. The textures of the three samples sandwiched in ITO cells, filled by capillary attraction from the isotropic liquid phase, were observed by POM of at various temperatures (Figs. S6, S8 and S10). All of compounds exhibited a typical fan-shaped texture in the SmA/B phase(s) as well as a spherulitic texture in the SmX phase. When the temperature was decreased from the

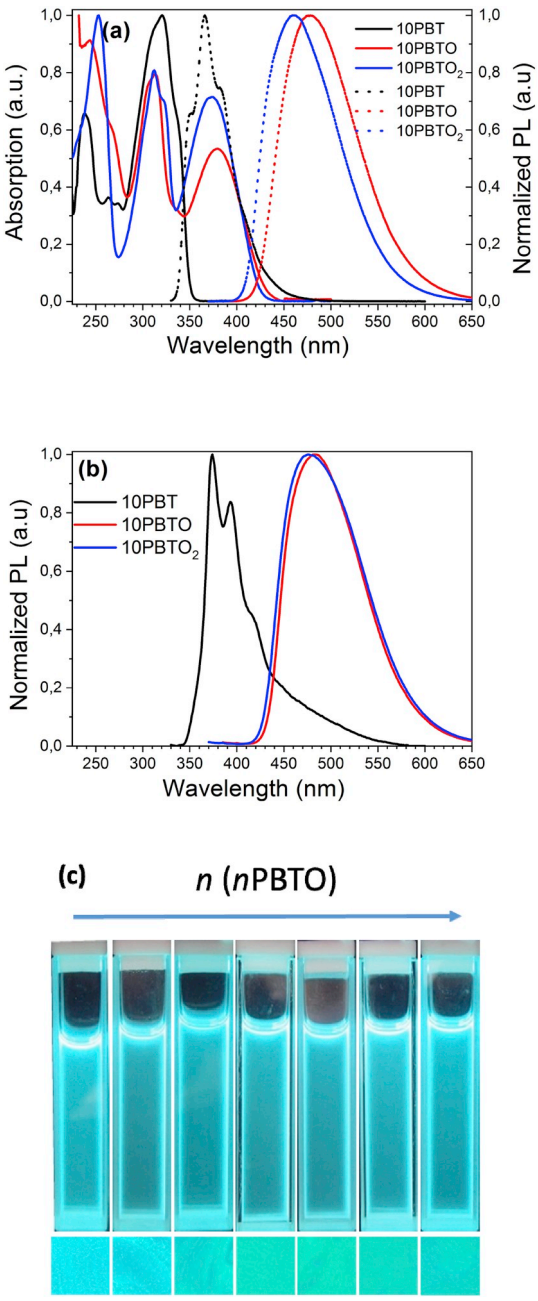

Fig. 5. (a) Normalized absorption (straight lines) and emission spectra (dotted lines) in micromolar THF solution obtained for 10PBT, 10PBTO and $10PBTO_2$ (chosen as representative compounds); (b) Normalized emission spectra of thin films of compounds 10PBT, 10PBTO and $10PBTO_2$. (c) Images of the micromolar THF solutions (top panel) and thin films (bottom panel) of *n*PBTO ($n = 4$–14) under UV light (365 nm).

isotropic to the crystalline phase, the POM images showed spherulitic texture with the presence of grain boundary on the substrate, which indicated that the molecules still retained the layer structure of the SmX phase in the crystalline phase. The charge carrier mobility was performed by TOF technique for the representative samples in a sandwich type ITO cell. The transient photocurrent measurements were performed on cooling at a very slow rate from the isotropic liquid to crystalline phase, at different temperatures with an applied electric field strength of 20000–50000 V cm^{-1}.

The double-logarithm plot of positive transport decay curves for 6PBT, 8PBT and 10PBT, respectively, showed in Fig. 6, enable the accurate read out of the transit time of charge carriers at various electric

Table 1
Photo-physical properties of the three decyl representative benzo[*b*]thiophene derivatives. Quantum yields (QY) were measured with solution concentration of 5×10^{-5} in THF excited at 310 nm (10PBT), at 365 nm (10PBTO) and at 350 nm ($10PBTO_2$). The data for the other compounds are in Table S3.

Mesogens	λ_{abs} (nm)	$\varepsilon \times 10^4$ ($L\,mol^{-1}cm^{-1}$)	λ_{em} (nm) solution	λ_{em} (nm) film	QY [%]
10PBT	238	1.28	350	374	50.8
	321	1.95	366	393	
			382		
10PBTO	244	1.83	478	483	41.9
	313	160			
	379	1.07			
$10PBTO_2$	252	2.00	459	476	62.6
	312	1.61			
	373	1.44			

field, thus proving that the transient photocurrent curves of three mesogens are non-dispersive. With the order degree of mesophase raised on cooling, the transit time of charge carriers decreased for all samples (Figs. S5, S7 and S9).

The positive charge carrier mobility of three mesogens is shown in the cooling process without electric field dependence (Fig. 6), while electron mobility was not observed. The hole transport of 6PBT shows mobilities in the order of $2 \times 10^{-4}\,cm^2\,V^{-1}\,s^{-1}$ in the isotropic liquid. In the SmA/SmB phase (~150 °C) the mobility rate increases to $5.5 \times 10^{-4}\,cm^2\,V^{-1}\,s^{-1}$, followed by a second sharp increase up to $4.2 \times 10^{-3}\,cm^2\,V^{-1}\,s^{-1}$ at the transition to SmX phase (142 °C). Meanwhile, the corresponding hole mobility values exhibited a slight temperature dependence both in the isotropic and smectic phases, it decreases very smoothly with the temperature falling. The charge carrier mobility in crystalline phase was not observed owing to cracks at domain boundaries. Similarly to 6PBT, the positive charge mobilities of 8PBT and 10PBT display lower values in the SmA phase than in the higher ordered SmX phase. The charge mobility of holes shows a slight dependence on the alkyl chain length, decreasing slowly with increasing length. These results are similar to several literature reported [49], both in discotic and calamitic molecules. In contrast, TOF measurements for the sulfoxide (PBTO) and sulfone ($PBTO_2$) derivatives did not yield any transit photo current.

The presence of this more ordered, low-temperature mesophase in the phase sequence, thus results in a significant improvement of the charge transport properties thanks to the pre-organizing templating effect of the SmA mesophase above, favoured by slow cooling [43].

3. Conclusion

We have successfully synthesized a series of benzothiophene-based liquid crystalline semiconductors and further oxidized derivatives from an abundant commercially available pharmaceutical precursory intermediate. The facile grafting of linear alkyl chains was indeed sufficient to promote the formation of smectic mesophases, showing the strong mesogenic character of this molecular species. The length of the alkyl chain and the degree of oxidation of the benzothiophene moiety were found to greatly influence the phase transition temperatures and thermal behaviour. Furthermore, the optical properties, emitting blue or yellow light with high quantum yields in the range of 38–62%, also are dramatically affected by the oxidation of the sulfur atom of the thiophene moiety. The charge carrier mobility of compound 6PBT measured by the photocurrent TOF technique revealed highest mobility range (about $4.2 \times 10^{-3}\,cm^2\,V^{-1}\,s^{-1}$) in the SmX phase, depending strongly on the order degree of the mesophase. Therefore, the utilization of this available pharmaceutical intermediate to design organic semiconducting and luminescent functional materials shows high promising applicative potentials, providing some additional structural molecular adjustments. For instance, PBT compounds have potential applications

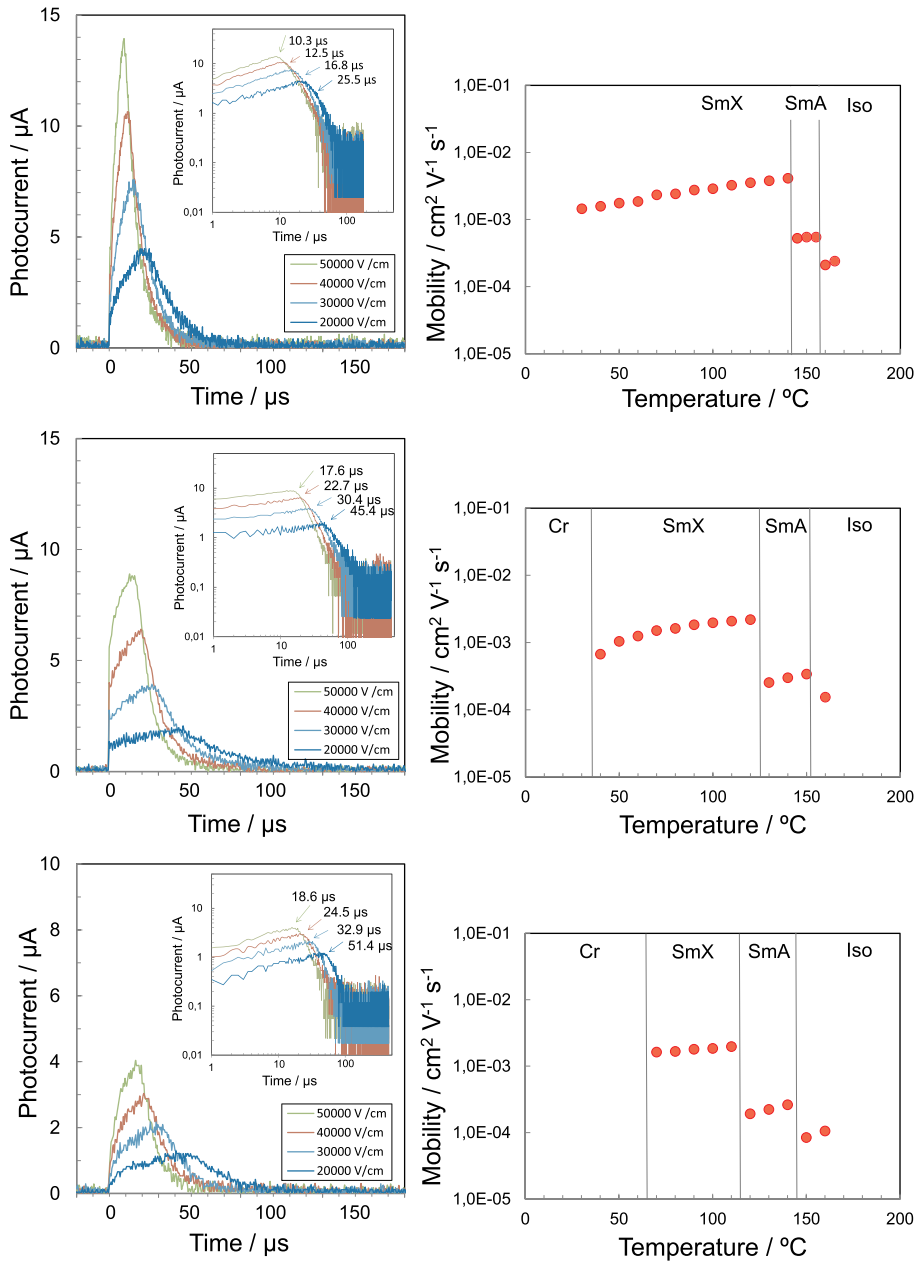

Fig. 6. Representative charge carrier mobility measured by the TOF technique. (Left) Electric field dependency of positive photocurrent decay curves (normal plot; Inset double-logarithm plot) at 120 °C (6PBT, with cell thickness is 17.7 µm), 100 °C (8PBT, with cell thickness is 17.7 µm) and 100 °C (10PBT, with cell thickness is 18.2 µm), from top to bottom. (Right) Temperature dependence of hole mobility (positive charge carrier transports), measured in the different phases on cooling for 6PBT (cell thickness is 17.7 µm), 8PBT (cell thickness is 17.7 µm) and 10PBT (cell thickness is 18.2 µm).

in the field of organic field-effect transistors (OFETs), as the TOF mobility results have been demonstrated, while PBTO and $PBTO_2$ derivatives can be used in fluorescent and light-emitting applications, as they emit blue and blue to green light, with mid-to-high quantum yields. The design of new mesogens based on 2-phenylbenzo[b]thiophene maybe be further improved by straightforward molecular derivatization, for example, through the substitution of the aromatic core by electron-donating or accepting groups, or by the extension of the molecular anisotropy and consequently enhanced π conjugation to boost the electronic properties. Moreover, the inclusion of such moieties into larger oligomeric, dendritic and polymeric structures would further facilitate their processing and incorporation into corresponding field-effect transistors and fluorescent sensors.

Supporting information

The file contains experimental techniques, synthetic details, POM images, DSC traces, SAXS patterns and indexation, UV–Vis and luminescence spectra, TOF tables, ^{1}H and ^{13}C NMR spectra and HMRS spectra.

Declaration of competing interest

The authors declare no conflict of interest.

Acknowledgements

This research was financially supported by the National Natural Science Foundation of China (NSFC, Fund numbers: 51773140, 21772135). KQZ and HM thank the support of NSFC-JSPS (Japan Society for the Promotion of Science, Joint Project 50811140156). BD and BH thank CNRS and University of Strasbourg for support.

Appendix A. Supplementary data

Supplementary data to this article can be found online at https://doi.

org/10.1016/j.dyepig.2019.107964.

References

[1] Keri RS, Chand K, Budagumpi S, Somappa SB, Patil SA, Nagaraja BM. Eur J Med Chem 2017;138:1002–33.
[2] Overk CR, Peng KW, Asghodom RT, Kastrati I, Lantvit DD, Qin Z, Frasor J, Bolton JL, Thatcher GR. ChemMedChem 2007;2:1520–6.
[3] Chang YS, Jeong JM, Lee YS, Kima HW, Rai G, Kim YJ, Lee DS, Chung J, Lee MC. Nucl Med Biol 2006;33:811–20.
[4] Mitchell WJ, Ferguson AJ, Kőse ME, Rupert BL, Ginley DS, Rumbles G, Shaheen SE, Kopidakis N. Chem Mater 2009;21:287–97.
[5] Vivas MG, Nogueira SL, Silva HS, Barbosa Neto NM, Marletta A, Serein-Spirau F, Lois S, Jarrosson T, Boni LD, Silva RA, Mendonca CR. J Phys Chem B 2011;115:12687–93.
[6] Fukazawa A, Oshima H, Shimizu S, Kobayashi N, Yamaguchi S. J Am Chem Soc 2014;136:8738–45.
[7] Wex B, Kaafarani BR, Danilov EO, Neckers DC. J Phys Chem A 2006;110:13754–8.
[8] Seki A, Funahashi M. Org Electron 2018;62:311–9.
[9] Liu Q, Gao X, Zhong H, Song J, Wang H. J Org Chem 2016;81:8612–6.
[10] Li, Zhao Y, Tan HS, Guo Y, Di CA, Yu G, Liu Y, Lin M, Lim SH, Zhou Y, Su H, Ong BS. Sci Rep 2012;2:754.
[11] Vollbrecht J, Oechsle P, Stepen A, Hoffmann F, Paradies J, Meyers T, Hilleringmann U, Schmidtke J, Kitzerow H. Org Electron 2018;61:266–75.
[12] Iino H, Hanna J. Polym J 2017;49:23–30.
[13] Takimiya K, Osaka I, Mori T, Nakano M. Acc Chem Res 2014;47:1493–502.
[14] Usta H, Facchetti A, Marks TJ. Acc Chem Res 2011;44:501–10.
[15] Jung KH, Kim KH, Lee DH, Jung DS, Park CE, Choi DH. Org Electron 2010;11:1584–93.
[16] Iino H, Hanna J. Mol Cryst Liq Cryst 2017;647:37–43.
[17] Monobe H, Kimoto M, Shimizu Y. Mol Cryst Liq Cryst 2016;629:181–6.
[18] Roche GH, Tsai YT, Clevers S, Thuau D, Castet F, Geerts YH, Moreau JJE, Wantz G, Dautel OJ. J Mater Chem C 2016;4:6742–9.
[19] Guo S, He Y, Murtaza I, Tan J, Pan J, Guo Y, Zhu Y, He Y, Meng H. Org Electron 2018;56:68–75.
[20] Ebata H, Izawa T, Miyazaki E, Takimiya K, Ikeda M, Kuwabara H, Yui T. J Am Chem Soc 2007;129:15732–3.
[21] He Y, Sezen M, Zhang D, Li A, Yan L, Yu H, He C, Goto O, Loo YL, Meng H. Adv Electron Mater 2016;2:1600179.
[22] Takimiya K, Ebata H, Sakamoto K, Izawa T, Otsubo T, Kunugi Y. J Am Chem Soc 2006;128:12604–5.
[23] Liu CX, Wang H, Du JQ, Zhao KQ, Hu P, Wang BQ, Monobe H, Heinrich B, Donnio B. J Mater Chem C 2018;6:4471–8.
[24] Monobe H, An L, Hu P, Wang BQ, Zhao KQ, Shimizu Y. Mol Cryst Liq Cryst 2017;647:119–26.
[25] Yang YS, Yasuda T, Kakizoe H, Mieno H, Kino H, Tateyama Y, Adachi C. Chem Commun 2013;49:6483–5.
[26] Amin AY, Khassanov A, Reuter K, Meyer-Friedrichsen T, Halik M. J Am Chem Soc 2012;134:16548–50.
[27] Minemawari H, Yamada T, Matsui H, Tsutsumi J, Haas S, Chiba R, Kumai R, Hasegawa T. Nature 2011;475:364–7.
[28] Oyama T, Mori T, Hashimoto T, Kamiya M, Ichikawa T, Komiyama H, Yang YS, Yasuda T. Adv Electron Mater 2018;4:1700390.
[29] Liu C, Minari T, Lu X, Kumatani A, Takimiya K, Tsukagoshi K. Adv Mater 2011;23:523–6.
[30] Iino H, Hanna J. Adv Mater 2011;23:1748–51.
[31] Chen C, Hernandez Maldonado D, Le Borgne D, Alary F, Lonetti B, Heinrich B, Donnio B, Moineau-Chane Ching KI. New J Chem 2016;40:7326–37.
[32] Mei J, Diao Y, Appleton AL, Fang L, Bao Z. J Am Chem Soc 2013;135:6724–46.
[33] Takimiya K, Shinamura S, Osaka I, Miyazaki E. Adv Mater 2011;23:4347–70.
[34] Oikawa K, Monobe H, Nakayama K, Kimoto T, Tsuchiya K, Heinrich B, Guillon D, Shimizu Y, Yokoyama M. Adv Mater 2007;19:1864–8.
[35] Funahashi M, Ishii T, Sonoda A. ChemPhysChem 2013;14:2750–8.
[36] van Breemen AJJM, Herwig PT, Chlon CHT, Sweelssen J, Schoo HFM, Setayesh S, Hardeman WM, Martin CA, de Leeuw DM, Valeton JJP, Bastiaansen CWM, Broer DJ, Popa-Merticaru AR, Meskers SCJ. J Am Chem Soc 2006;128:2336–45.
[37] Shimizu Y, Oikawa K, Nakayama K, Guillon D. J Mater Chem 2007;17:4223–9.
[38] Liau WL, Su YJ, Tseng HF, Chen JT, Hsu CS. Liq Cryst 2017;44:557–65.
[39] Kurfürst M, Kozmík V, Svoboda J, Novotná V, Glogarová M. Liq Cryst 2008;35:21–31.
[40] Kozmík V, Henke A, Řehová L, Kurfürst M, Slabochová M, Svoboda J, Novotná V, Glogarová M. Liq Cryst 2011;38:1245–61.
[41] Kozmík V, Hodík T, Svoboda J, Novotná V, Pociecha D, Gorecka E. Liq Cryst 2016;43:839–52.
[42] Xiong R, Patel HK, Gutgesell LM, Zhao J, Delgado-Rivera L, Pham TN, Zhao H, Carlson K, Martin T, Katzenellenbogen JA, Moore TW, Tonetti DA, Thatcher GR. J Med Chem 2016;59:219–37.
[43] Lincker F, Attias A-J, Mathevet F, Heinrich B, Donnio B, Fave J-L, Rannou P, Demadrille R. Chem Commun 2012;48:3209–11.
[44] Zhao KQ, Jing M, An LL, Du JQ, Wang YH, Hu P, Wang BQ, Monobe H, Heinrich B, Donnio B. J Mater Chem C 2017;5:669–82.
[45] Pouzet P, Erdelmeier I, Ginderow D, Mornon JP, Dansette PM, Mansuy D. J Heterocycl Chem 1997;34:1567–74.
[46] Reddy KR, Varathan E, Lobo NP, Easwaramoorthi S, Narasimhaswamy T. J Phys Chem C 2016;120:22257–69.
[47] He K, Li W, Tian H, Zhang J, Yan D, Geng Y, Wang F. ACS Appl Mater Interfaces 2017;9:35427–36.
[48] Seed AJ, Toyne KJ, Goodby JW, Hird M. J Mater Chem 2000;10:2069–80.
[49] Yang Y, Wang H, Wang HF, Liu CX, Zhao KQ, Wang BQ, Hu P, Monobe H, Heinrich B, Donnio B. Cryst Growth Des 2018;18:4296–305.